ATLANTIS PRESS

Advances in Computer Science Research, volume 58

Modeling, Simulation and Optimization Technologies and Applications (MSOTA 2016)

Parameter Optimization of Surface Textures of Oil-lubricated Journal Bearings

Yongfang Zhang[1,2,*], Jingqun Zhao[1,2], Liangjun Xiao[1,2], Xianwei Li[1,2] and Yanjun Lu[3]

[1]School of Printing, Packaging Engineering and Digital Media Technology, Xi'an University of Technology, Xi'an, China

[2]State Key Laboratory for Strength and Vibration of Mechanical Structures, Xi'an Jiaotong University, Xi'an, China

[3]School of Mechanical and Precision Instrument Engineering, Xi'an University of Technology, Xi'an, China

***Abstract*—The effects of sphere dimples on the tribological performances of the journal bearing were investigated. The oil film rupture and reformation positions were obtained using a mass-conservation JFO（Jakobsson, Floberg, Olsson）boundary condition. The influences of the sphere dimples with various distribution forms and geometry parameters on the load-carrying capacity and friction characteristics were investigated. On this basis, parameter optimization of textured sphere dimples was implemented using genetic algorithm. The results show that the optimal dimple angle range and maximum depth can increase load-carrying capacity and decrease friction factor effectively when the eccentricity is small, but the sphere dimple texture is invalid for the decrease of friction factor when the eccentricity is large.**

Keywords-surface texture; load-carrying capacity; friction factor; genetic optimization

I. INTRODUCTION

The oil-lubricated journal bearings have been widely used in rotary machines such as conductors and generators due to their high stability and low friction. It is important to enhance the load-carrying capacity and reduce the friction of journal bearings because they usually run under high-speed and heavy-load conditions. The surface texture has been adopted to improve the tribological properties of journal bearings with the different shape, size and distribution form of texture. Meanwhile, the texture parameters can be optimized to maximize the load-carrying capacity and minimize the friction factor. The surface texture of journal bearings have been applied to improve the tribological properties of bearings since last two decades. Adatepe et al. investigated the tribological behaviors of non-grooved and micro-grooved journal bearings under dynamic loading [1]. The results showed that the micro-grooved shapes have a great influence on the bearing performance improvement and the appropriate parameters of texture is beneficial to improve tribological performance of journal bearings. Rao et al. applied modified classical Reynolds equation to study the effect of texture on improvement in load capacity and reduction in coefficient of friction for partially textured journal bearing [2]. Tala-Ighil et al. investigated the effect of the appropriate surface texture geometry and right texture distribution on the hydrodynamic characteristics improvement of the fully textured and partially textured journal bearings [3].

In order to improve the load-carrying capacity and reduce the friction, more attentions have been paid to optimization of texture parameters. Papadopoulos et al. presented an optimization approach based on genetic algorithms to obtain the optimal texturing patterns to improve the load-carrying capacity of micro-thrust bearings in a wide range of convergence ratios [4]. Zhou et al. studied the effects of the texturing parameters on the load carrying capacity and film thickness under different velocities, and obtained the ranges of optimum texturing parameters [5]. In this paper, the effects of sphere dimples with different start angles, maximum depths and area ratios on the load-carrying capacity and friction factor of oil-lubricated journal bearing are studied. The start angle and maximum depth are optimized using genetic algorithm.

II. THEORETICAL ANALYSIS

A. Lubrication Control Equation and Boundary Conditions

Figure 1 shows schematic diagram of journal bearing. In Figure 1, Ob is the bearing center, Oj is the journal center, ϕ is the angle from the negative direction of the y axis to oil film position, φ is the angle which goes from the deviation line to oil film position, θ is the deviation angle, e is the eccentricity, r is the journal radius, R is bearing radius, ω is the angular velocity of journal, h is the oil film thickness, fr and ft are the radial and tangential oil film forces respectively, fx and fy are the oil film forces in negative x and y directions, φs is the circumferential start angle of texture region which goes from the deviation line, κ is the circumferential range angle of texture region. In Figure 2, B is the bearing width.

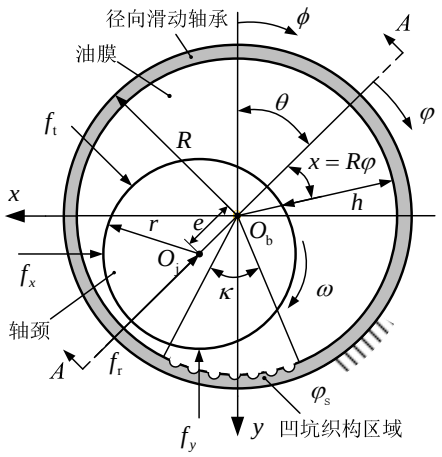

FIGURE I. SCHEMATIC DIAGRAM OF OIL-LUBRICATED JOURNAL BEARING.

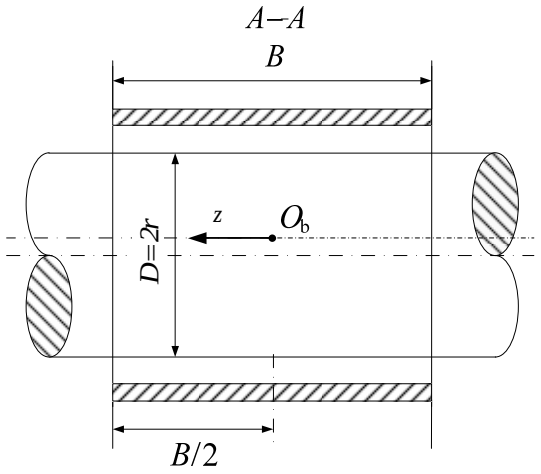

FIGURE II. THE CROSS SECTION OF OIL-LUBRICATED JOURNAL BEARING.

The average Reynolds equation based on the assumptions of laminar, isothermal and incompressible Newton fluid lubrication can be expressed as

$$\frac{\partial}{\partial\varphi}(\phi_1\frac{h^3}{\mu}\frac{\partial p}{\partial\varphi})+R^2\frac{\partial}{\partial z}(\phi_2\frac{h^3}{\mu}\frac{\partial p}{\partial z})=6U\phi_{con}R\frac{\partial h}{\partial\varphi}+6U\sigma R\frac{\partial\phi_s}{\partial\varphi} \quad (1)$$

where z is the axial coordinate, p is the oil film pressure, μ is the dynamic viscosity, σ is the surface roughness, U is the circumferential velocity of journal, ϕ1 and ϕ2 are pressure flow factors in the circumferential and axial directions respectively, ϕcon is the contact factor, and ϕs is the flow shear factor.

Based on the mass-conservation JFO (Jakobsson, Floberg, Olsson) theory, the lubrication region of oil film can be divided into the whole film area and the cavitation area. The lubrication performance of the whole film area can be described in (1). The lubrication control equation of the cavitation area can be written as

$$U\rho_c\phi_{con}\frac{\partial h}{\partial\varphi}+U\sigma\frac{\partial(\rho_c\phi_s)}{\partial\varphi}=0 \quad (2)$$

where ρc is the oil film density in the cavitation area.

The boundary condition of oil film pressure distribution is

$$\begin{cases} p(\varphi,\pm\frac{B}{2})=0 \\ p(\varphi,z)=p(\varphi+2\pi,\ z) \end{cases} \quad (3)$$

The pressure distribution of oil film rupture boundary satisfies the cavitation boundary conditions.

$$\begin{cases} p=p_c \\ \frac{\partial p}{\partial n}=0 \end{cases} \quad (4)$$

where n is the normal of oil film rupture.

The pressure distribution on the boundary of oil film reformation satisfies the mass-conservation JFO.

$$\frac{h^2}{12\mu}\frac{\partial p}{\partial n}=\frac{v_n}{2}(1-\frac{\rho}{\rho_c}) \quad (5)$$

where vn is the normal velocity of oil film.

In order to solve the lubrication control equations of the whole film area and cavitation area simultaneously, the switch function g and cavitation index α are defined as

$$g=\begin{cases} 0 & (\alpha<0) \\ 1 & (\alpha\geq 0) \end{cases} \quad (6)$$

$$\alpha=\begin{cases} -1+\frac{\rho_c}{\rho} & \text{（cavitation area）} \\ \frac{p-p_c}{p_a} & \text{（whole film area）} \end{cases} \quad (7)$$

where pa is the atmospheric pressure.

Substituting (6) and (7) into (1) and (2), the unified lubrication control equation can be obtained to deal with the whole area and the cavitation area simultaneously.

$$\begin{aligned} &\frac{\partial}{\partial\varphi}(\phi_1\frac{p_a h^3}{\mu}\frac{\partial(\alpha g)}{\partial\varphi})+R^2\frac{\partial}{\partial z}(\phi_2\frac{p_a h^3}{\mu}\frac{\partial(\alpha g)}{\partial z}) \\ &=6U\phi_{con}[1+(1-g)\alpha]R\frac{\partial h}{\partial\varphi}+6U\sigma R\frac{\partial\{[1+(1-g)\alpha]\phi_s\}}{\partial\varphi} \end{aligned} \quad (8)$$

B. Oil Film Thickness Equation

Figure 3 shows schematic diagram of sphere dimple. In Figure 3, rd and hd are the radius and maximum depth of dimple, ξοη is the local coordinate system of dimpled unit. The area density of sphere dimple can be expresed as

$$s=\pi r_d^2/l_{cell}^2 \quad (9)$$

where lcell is the length of square unit.

The oil film thickness of journal bearing with the sphere dimples at the arbitrary position can be expressed as

$$h=\begin{cases} c(1+\varepsilon\cos\varphi) & (\varphi,z)\notin\Omega \\ c(1+\varepsilon\cos\varphi)+h_t & (\varphi,z)\in\Omega \end{cases} \quad (10)$$

where

$$h_t=\sqrt{(\frac{r_d^2+h_d^2}{2h_d})^2-(\xi^2+\eta^2)}-\frac{r_d^2-h_d^2}{2h_d}.$$

C. Load-Carrying Capacity and Friction Factor

The load-carrying capacity Wa of asperity, and actual contact area Acon based on Greenwood-Tripp model can be written as

$$W_a = \frac{16\sqrt{2}}{15}\pi(\vartheta\beta\sigma)^2 E'\sqrt{\sigma/\beta}AF_{2.5}(h/\sigma) \tag{11}$$

$$A_{con} = \pi^2(\vartheta\beta\sigma)^2 F_2(h/\sigma) \tag{12}$$

$$F_n(h/\sigma) = \frac{1}{\sqrt{2\pi}}\int_{h/\sigma}^{\infty}(s-h/\sigma)^n e^{-s^2/2}\mathrm{d}s \tag{13}$$

where A is the contact area, E′ is the composite elastic modulus, ϑ is density of asperity, and β is the radius of curvature of asperity.

The total friction force Ff is composed of the adhesive shear force Fh of oil film and the contact shear force Fa of asperity under the mixed lubrication condition. The total friction force can be written as

$$F_f = F_h + F_a \tag{14}$$

$$F_a = \tau_0 A_{con} + \alpha_0 W_a \tag{15}$$

$$F_h = \iint_{A_1}\frac{\mu U}{h}[(\varphi_f - \varphi_{fs}) + 2V_{r1}\varphi_{fs}]\mathrm{d}x\mathrm{d}y \tag{16}$$

where A1 is the actual area of oil film, φf and φfs are the shear force factors, τ0=2×106 is the shear force constant, and α0=0.1 is the boundary friction coefficient.

The oil film forces in the radial and tangential directions can be expressed as

$$\begin{cases} F_r = -\iint_{\Omega_1} p\cos\varphi\mathrm{d}\varphi\mathrm{d}\lambda \\ F_t = -\iint_{\Omega_1} p\sin\varphi\mathrm{d}\varphi\mathrm{d}\lambda \end{cases} \tag{17}$$

where Ω1 is the oil film area.

The oil film forces along negative x and y axis are

$$\begin{cases} F_x = F_t\cos\theta + F_r\sin\theta \\ F_y = -F_t\sin\theta + F_r\cos\theta \end{cases}. \tag{18}$$

The oil film force F and load-carrying capacity W are

$$F = \sqrt{F_x^2 + F_y^2} \tag{19}$$

$$W = F + W_a\,. \tag{20}$$

The friction factor can be expressed as

$$f = F_f / W\,. \tag{21}$$

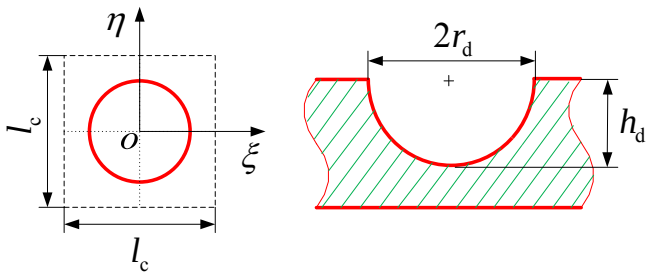

FIGURE III. SCHEMATIC DIAGRAM OF SPHERE DIMPLE.

III. RESULTS AND DISCUSSIONS

The geometric parameters of journal bearing are: the width of the bearing B=20mm, the radius clearance c=0.04mm, the roughness σ1=σ2=0.4μm, r=32.5mm, the rotational speed n=2200r/min, and μ=0.03Pa·s. Figure 4 shows the dimensionless load-carrying capacity W versus the start angle of texture area φs for various circumferential range angles of texture area. As shown in Figure 4, the dimensionless load-carrying capacity decreases and then increases with the increase of circumferential range angle of texture area, and the load-carrying capacity is maximum when φs=60º and κ=30º. Figure 5 shows the friction factor f versus the start angle of texture area φs for various circumferential range angles of texture area. As shown in Figure 5, the friction factor increases with the increase of the start angle, and the friction factor is minimum when φs=0º and κ=90º. Figure 6 shows the dimensionless load-carrying capacity W versus the area density s for different dimple number. As shown in Figure 6, the dimensionless load-carrying capacity is an increasing function of the area density of dimples, and the effect of dimple number on the load-carrying capacity is limited. Figure 7 shows the dimensionless load-carrying capacity W versus the maximum depth hd for different dimple number. As shown in Figure 7, the dimensionless load-carrying capacity increases and then decreases with the maximum depth. Figure 8 shows the friction factor f versus the area density s for different dimple number. As shown in Figure 8, the friction factor is a decreasing function of the area density of dimples and larger area density has little influence on the friction factor. Figure 9 shows the friction factor f versus the maximum depth hd for different dimple number. As shown in Figure 9, the friction factor decreases and then increases with the increase of the texture depth.

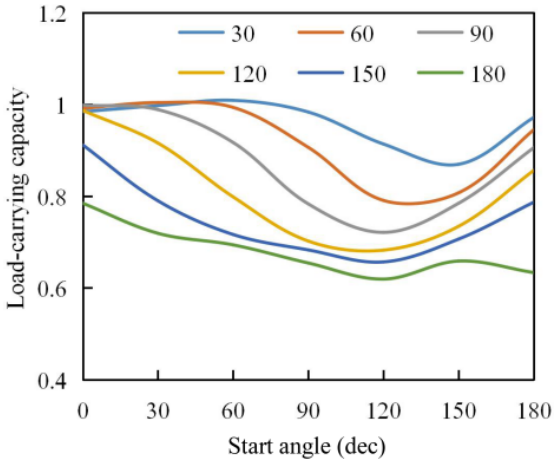

FIGURE IV. THE DIMENSIONLESS LOAD-CARRYING CAPACITY W VERSUS THE START ANGLE ΦS FOR VARIOUS CIRCUMFERENTIAL RANGE ANGLES OF TEXTURE AREA.

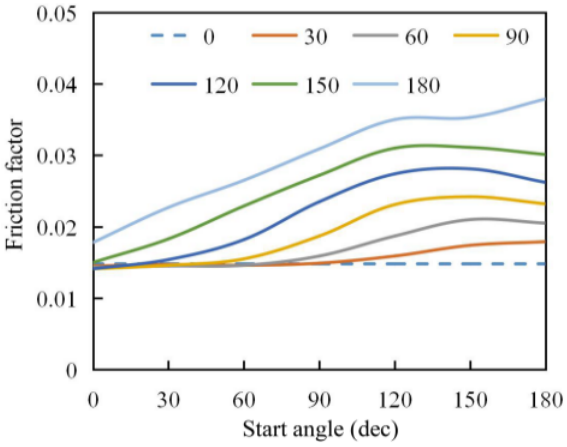

FIGURE V. THE FRICTION FACTOR F VERSUS THE START ANGLE ΦS FOR VARIOUS CIRCUMFERENTIAL ANGLE RANGES OF TEXTURE AREA.

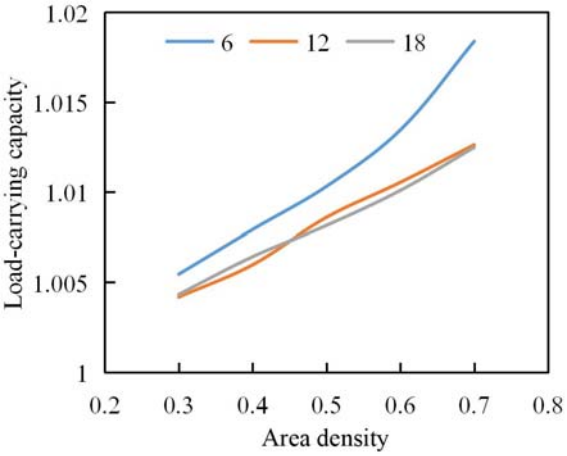

FIGURE VI. THE DIMENSIONLESS LOAD-CARRYING CAPACITY W VERSUS THE AREA DENSITY S FOR DIFFERENT DIMPLE NUMBER.

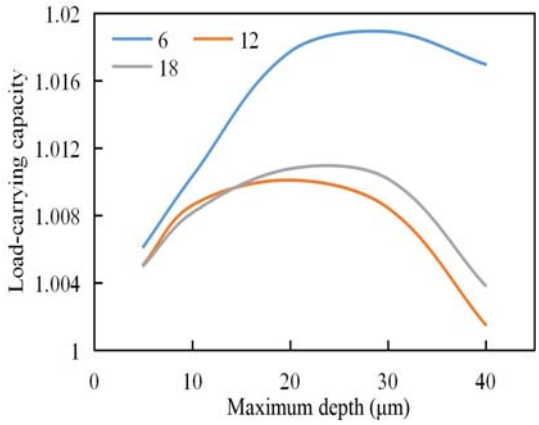

FIGURE VII. THE DIMENSIONLESS LOAD-CARRYING CAPACITY W VERSUS THEMAXIMUM DEPTH HD FOR DIFFERENT DIMPLE NUMBER.

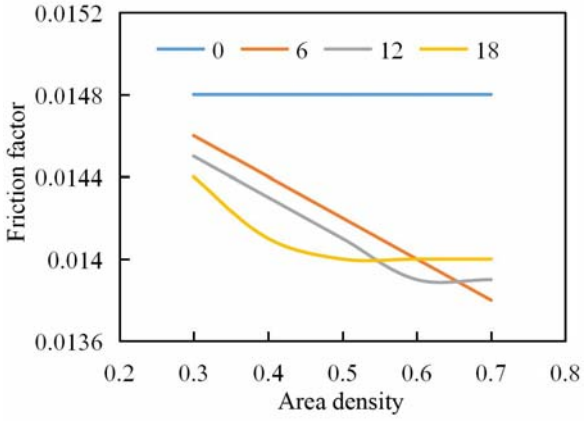

FIGURE VIII. THE FRICTION FACTOR F VERSUS THE AREA DENSITY S FOR DIFFERENT DIMPLE NUMBER.

IV. OPTIMUM TEXTURE PARAMETER

The parameter optimization of surface texture is to find the maximum load-carrying capacity and minimum friction factor using genetic algorithm. The optimal parameters of sphere dimples which maximize the load-carrying capacity of journal bearing are obtained when κ=29.61° and hd=33.35μm (φs=60°).

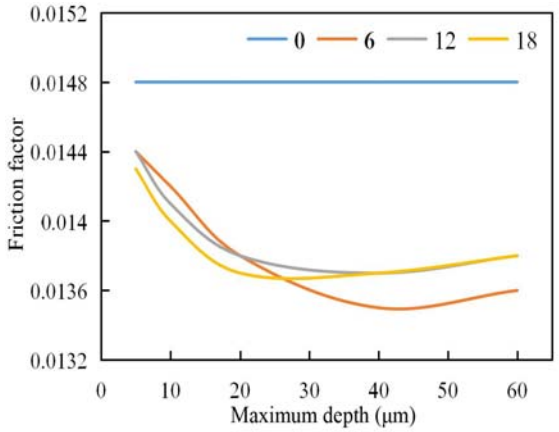

FIGURE IX. THE FRICTION FACTOR F VERSUS THE MAXIMUM DEPTH HDFOR DIFFERENT DIMPLE NUMBER.

The dimensionless load-carrying capacity of non-dimpled bearing is 1, but the dimensionless load-carrying capacity is 1.24 after the parameters optimization of texture. The optimal parameters of sphere dimples which minimize the friction factor are obtained when κ=115.52º and hd=45.74μm (φs=0º).

V. CONCLUSIONS

The load-carrying capacity and friction factor of sphere dimples are investigated and the texture parameters, such as circumferential range angle of texture area and maximum depth are optimized. The numerical results show that the optimal circumferential range angle, maximum depth of sphere dimples etc. can maximize the load-carrying capacity and minimize the friction factor. The load-carrying capacity is an increasing function of area density of texture, and the friction factor is a decreasing function of area density of texture. Besides, the effect of dimple number on the load-carrying capacity and friction factor is limited.

ACKNOWLEDGMENT

This work is supported by Natural Science Foundation of China (Grant No. 51375380), Open Project of State Key Laboratory for Strength and Vibration of Mechanical Structures (Grant No. SV2016-KF-10), National Natural Science Foundation of Shaanxi Province of China (Grant No. 2014JM2-5082), Scientific Research Program of Shaanxi Provincial Education Department of China (Grant No. 15JS068).

REFERENCES

[1] H. Adatepe, A. Bıyıklıoglu, and H. Sofuoglu, "An investigation of tribological behaviors of dynamically loaded non-grooved and micro-grooved journal bearings," Tribol. Int. Oxford, vol. 58, pp. 12-19, February 2013.

[2] T. V. V. L. N. Rao, A. M. A. Rani, T. Nagarajan, and F. M. Hashim, "Analysis of slider and journal bearing using partially textured slip surface," Tribol. Int. Oxford, vol. 56, pp. 121-128, December 2012.

[3] N. Tala-Ighil, and M. Fillon, "A numerical investigation of both thermal and texturing surface effects on the journal bearings static characteristics," Tribol. Int. Oxford, vol. 90, pp. 228-239, October 2015.

[4] C. I. Papadopoulos, E. E. Efstathiou, P. G. Nikolakopoulos, and L. Kaiktsis, "Geometry optimization of textured three-dimensional micro-thrust bearings," J. Tribol. New York, vol. 133, pp. 041702, October 2011.

[5] Y. K. Zhou, H. Zhu, W. Tang, C. B. Ma, and W. Q. Zhang, "Development of the theoretical model for the optimal design of surface texturing on cylinder liner," Tribol. Int. Oxford, vol. 52, pp. 1-6, August 2012.